Available online at www.sciencedirect.com
SCIENCE DIRECT®
Journal of Molecular Structure 691 (2004) 241–248
Journal of MOLECULAR STRUCTURE
www.elsevier.com/locate/molstruc

Experimental and computational studies of the structure and vibrational spectra of 4-dimethylamino pyridinium-betaine of squaric acid

Tsonko M. Kolev*, Bistra A. Stamboliyska, Denitsa Y. Yancheva, Venelin Enchev

Institute of Organic Chemistry, Bulgarian Academy of Sciences, Acad G. Bontchev Str. Bl. 9, 1113 Sofia, Bulgaria

Received 12 September 2003; revised 17 December 2003; accepted 18 December 2003

Abstract

The FTIR spectra of 4-dimethylamino pyridinium-betaine of squaric acid in 4000–100 cm^{-1} frequency region in solid state were measured. In addition, the structure and harmonic vibrational frequencies of this molecule were theoretically evaluated using restricted Hartree–Fock and B3LYP density functional methods. The computed vibrational frequencies are used to determine the types of molecular motions associated with each of the experimental bands observed. The results of the optimized molecular structure obtained on the basis of restricted Hartree–Fock and density functional theory calculations are presented and compared with the experimental X-ray diffraction data for the 4-dimethylamino pyridinium-betaine of squaric acid single crystal. Comparison with the experimental spectra provides important information about the ability of these computational methods to describe the vibrational modes in these highly polar strained ring compounds.

Keywords: 4-Dimethylamino pyridinium-betaine of squaric acid; Vibrational spectra; Ab initio force field; Electronic structure; Band assignment

1. Introduction

Organic systems with second- and third order nonlinear optical (NLO) properties have been intensively studied due to their potential applications such as second harmonic generation, optical parametric oscillation, electro-optic modulation [1–3]. In the recent years different application of NLO and photorefractive (PR) materials have been developed—e.g. optical frequencies conversion, dynamic holography optical writing and optical guiding of laser beam. It is known that certain classes of organic compounds show very high NLO and electro-optical effects [4–6]. The linearity is based on molecular units, containing strongly delocalised π-electron system with donor and acceptor groups at the opposite ends of the molecule. Among these materials the substituted betaines play important role because of its dipolar structure [7,8].

We have reported a study of the IR spectra of unsubstituted pyridinium-betaine of squaric acid [9] and evaluated the quality of the prediction provided by quantum chemical calculations using restricted HF and density functional theory (DFT) methods. The chemistry of some substituted pyridinium betaines of squaric acid was described by Schmidt et al. [10–12]. The authors have published only four characteristic bands in IR spectra of the compounds. We have studied the UV–Vis spectra of representative series of 3- and 4-substituted compounds of this class [13]. As a result of this elucidation was established the clearly distinct negative solvatochromism, characteristic for compounds with dipolar electronic ground state structure. The two absorption bands in the visible region have shown charge transfer character, which determine their strong dependence on medium polarity and substituent nature. The investigation of the spectral behavior of the 4-dimethylamino pyridinium-betaine of squaric acid (DAPB) and some other representatives has revealed their potential NLO and electro-optical properties. Furthermore, this compound exhibits remarkable thermal stability, required for these applications.

In the present paper, we report the experimental FTIR spectra in solid state and in nujol mulls and the result from the ab initio and DFT calculations on the electronic structure and vibrational spectra of DAPB. To our knowledge, infrared spectra for DAPB have not been reported. Assignment of fundamental molecular vibrations is made with

* Corresponding author. Tel.: +359-2-9606-106; fax: +359-2-8700-225.
E-mail address: kolev@orgchm.bas.bg (T.M. Kolev).

0022-2860/$ - see front matter © 2003 Elsevier B.V. All rights reserved.
doi:10.1016/j.molstruc.2003.12.033

the help of quantum chemical calculations. Comparisons were made between calculated and observed IR spectra, and calculated geometry with published X-ray crystallographic data.

2. Experimental

The preparation of DAPB is described in Ref. [10]. The product is purified by double recrystallization from water and DMSO. The melting point, determined by means of differential scanning calorimetry (DSC)—393–395 °C of the compound studied is considerably higher than this published in the literature [12]. The crystals are very stable under normal conditions. The IR spectra of the compound studied were recorded in KBr and CsI pellets as well as in nujol and perdeuteronujol mulls on a Bruker IFS-113v spectrometer equipped with high intensity Globar source, Ge/KBr beam splitter, and DTGS detector. The far IR spectra have been recorded on the same spectrometer equipped with high-pressure Hg arc lamp a 6.25 and 25 μm Mylar beam splitter and DTGS detector. In both cases, the spectra have been recorded at a resolution of 1 cm^{-1} (100 scans).

3. Computations

Ab initio restricted Hartree–Fock (RHF) method and DFT are used to obtain equilibrium geometry, force field and fundamental vibrational frequency of DAPB molecule. All calculations have been performed with the standard GAUSSIAN [14] software (AIX, version 1998). DFT method, employed in the present study is B3LYP—Becke's three-parameter hybrid method [15] using the correlation functional of Lee, Yang and Parr [16]. The standard 6-31G* basis set was applied in all calculations. The local minimum was verified by establishing that the matrix of the energy second derivatives (Hessian) has no negative eigenvalues. The standard analytical procedure, implemented in GAUSSIAN was used. It is well known that both RHF and B3LYP methods overestimate the frequencies of fundamental vibrations significantly. Thus, for a better correspondence between experimental and calculated values, the RHF and B3LYP results were modified using the empirical scaling factor, reported by Scott and Radom [17].

4. Results and discussion

4.1. Structural analysis

4.1.1. Geometries

X-ray crystallographic data for DAPB were provided by Kolev et al. [18]. The molecules in the crystal structure are held together by means of intermolecular nonclassical hydrogen bonds formed by methyl groups and O-atom of the 'pure' carbonyl group of adjacent molecule (dist. 3.417(2) Å), which link the molecules in the crystal into infinite chains. The intramolecular hydrogen bonds formed by O-atom of the C–O groups and H-atoms at positions 2 and 6 in the pyridinium ring (3.223(2) Å) contribute to the extremely high melting point of the compound [18]. The title compound can be considered as being essentially planar from experiment (maximum deviation from planarity 0.077(2) Å). The molecular geometry lies between the resonance structures shown in the chemical diagrams (Scheme 1).

The optimized geometry parameters, i.e. bond lengths and bond angles, computed by RHF and DFT methods are compared with X-ray data [18] in Table 1. The numbering of the atoms in DAPB is shown in Scheme 2. In both computation methods C_{2v} symmetry for DAPB molecule has been taken into account. As can be seen there is a good agreement between experimental and theoretical geometry parameters. Both RHF and B3LYP predict that the $C_{10}-O_{17}$ bond is with 0.025 Å shorter than the equalized C_8-O_{16} and C_9-O_{17} bonds and this agrees with the experimental measurements. It is interesting to note that RHF/6-31G* underestimates the C=O and C⁼⁼O bond lengths by 0.027 and 0.029 Å, respectively, while the B3LYP/6-31G predicts these bond distances quite accurately and the calculated

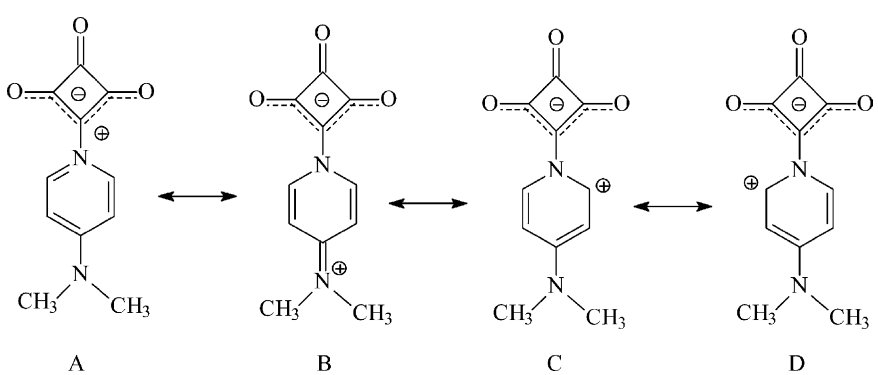

Scheme 1. Resonance contributors A, B, C, and D of DAPB.

Table 1
Experimental and calculated bond lengths (Å) and bond angles (°) of the DAPB molecule

Sructural parameters[a]	Experimental[b]	B3LYP/6-31G*	RHF/6-31G*
N^1-C^2	1.369	1.368	1.345
C^2-C^3	1.346	1.372	1.360
C^3-C^4	1.416	1.422	1.415
N^1-C^7	1.400	1.394	1.410
C^8-C^7	1.421	1.436	1.416
C^8-C^{10}	1.513	1.569	1.544
C^8-O^{16}	1.231	1.226	1.204
$C^{10}-O^{17}$	1.207	1.201	1.179
C^4-N^{13}	1.335	1.361	1.344
$N^{13}-C^{19}$	1.469	1.459	1.455
m.d.[c]		0.017	0.018
$\langle(N^1C^2C^3)$	121.9	121.14	121.7
$\langle(C^2C^3C^4)$	121.0	120.9	120.4
$\langle(C^3C^4N^{13})$	122.0	121.9	121.9
$\langle(C^3C^4C^5)$	115.9	116.1	116.0
$\langle(C^4N^{13}C^{19})$	121.4	120.3	121.3
$\langle(C^7N^1C^2)$	120.9	120.1	120.2
$\langle(C^{10}C^8C^7)$	88.1	87.4	87.3
$\langle(C^8C^7C^1)$	132.2	131.1	131.1
$\langle(C^8C^7C^9)$	95.6	97.8	97.9
$\langle(O^{17}C^{10}C^8)$	135.9	136.4	136.2
$\langle(O^{16}C^8C^7)$	136.4	135.1	136.1
$\langle(C^{19}N^{13}C^{20})$	117.1	119.6	119.3
m.d.[c]		1.03	0.8

[a] Numberimg of atoms as in Scheme 2.
[b] Ref. [18].
[c] Mean absolute deviation between experimental and calculated data.

deviations for the same lengths are only 0.005 Å. The interatomic distance $N-C_7 = 1.400$ Å (exp.) is predicted very well from the both theoretical methods (deviations are 0.006 and 0.010 Å calculated by means of B3LYP and RHF, respectively. The most surprising is the bond distance $C_4-N_{13} = 1.335$ Å (exp.), while the both theoretical methods predict a longer bond length (Table 1). This distance is the shortest among all distances around the substituted pyridinium ring. The X-ray crystallographic observations indicated that the double bonds in the pyridinium ring of

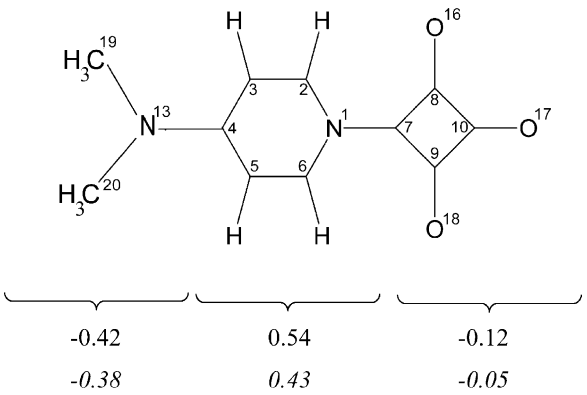

Scheme 2. The RHF and B3LYP (in italics) net electronic charges over Py- and Sq- and $N(CH_3)$ fragments of DAPB molecule.

DAPB are localized on C_2-C_3 and C_5-C_6 while the bonds N_1-C_2 (resp. N_1-C_6) and C_3-C_4 (resp. C_5-C_4) are some longer. Similar quinoid features were also observed in the X-ray diffraction study [19] for the molecular geometry of 4-dimethylamino pyridinium derivatives. This bond length alternation in the pyridinium ring is not consistent by the quantum-chemical calculations. Both computational methods predict the bond angles quite accurately and the calculated mean deviations for RHF and B3LYP are 1.0 and 0.8°, respectively.

4.1.2. Electronic structure

The calculated electronic charges are listed in Table 2. The potential nonlinearity of DAPB, suggested by two charge transfer bands in its UV–Vis spectrum showing noticeable negative solvatohromism [13] as well as by its crystal structure [18], is due to the charge transfer between the positively charged pyridinium ring and the negatively charged Sq moiety and slightly negatively charged dimethylamino group (Scheme 2).

The dipole moment of DMPB is 16.1 D calculated by means of B3LYP and 17.1 D with help of RHF. In accordance to this is the extremely high decomposition point at 393–395 °C determined through DSC. The comparison between the electronic charges of the studied

Table 2
Net electronic charges (Q) over atoms of DAPB molecule

Atom[a]	Q	
	B3LYP	RHF
N_1	−0.50	−0.73
C_2	0.08	0.16
C_3	−0.24	−0.36
C_4	0.42	0.51
C_5	−0.23	−0.36
C_6	0.08	0.16
C_7	0.15	0.03
C_8	0.31	0.44
C_9	0.31	0.44
C_{10}	0.34	0.44
H_{11}	0.24	0.33
H_{12}	0.17	0.25
N_{13}	−0.47	−0.70
H_{14}	0.17	0.25
H_{15}	0.24	0.33
O_{16}	−0.53	−0.64
O_{17}	−0.43	−0.50
O_{18}	−0.53	−0.64
C_{19}	−0.33	−0.30
C_{20}	−0.33	−0.30
H_{21}	0.18	0.19
H_{22}	0.18	0.20
H_{23}	0.18	0.20
H_{24}	0.18	0.20
H_{25}	0.18	0.20
H_{26}	0.18	0.20

[a] For atom numbering see Scheme 2.

molecule and these ones of PBSQ [9] shows that the unsubstituted molecule excels DAPB as push–pull system. The explanation of this fact is the presence of dymethylamino group which increases the dipole moment of DAPB but strongly decreases the positive charge over the *N*-pyridinium atom. In the previous paper [9] it was found that the charge flux in PBSQ (intramolecular charge transfer or CT) creates a large permanent dipole moment (11.16 D (B3LYP/6-31G*) and 12.56 D (RHF/6-31G)), whereas in DAPB the dipole moment is greater. Thus, it can be expected that the molecule studied is a typical dipolar one but its first hyperpolarizability will be smaller.

4.2. Vibrational assignment

The fragment of the IR spectrum of DAPB in 3200–2000 cm^{-1} in KBr pellet is shown in Fig. 1. The middle IR spectrum of the same compound in KBr disc is shown in Fig. 2. The FTIR spectrum in 400–100 cm^{-1} in CsI matrix of DAPB is shown in Fig. 3. The numeric values of experimental frequencies are compared with the corresponding RHF/6-31G* and B3LYP/6-31G* ones in Table 3. The computed vibrational frequencies are used to determine the types of molecular motions associated with each of the observed experimental bands. The assignment of the vibrational bands of the pyridinium moiety is denoted by Py, the dimethylamino part by Me and that one of squarate is designated by Sq. Wilson's notation [20] is employed. As it can be seen from Table 3, the agreement of the calculated frequencies with the experimental data is very good. The mean absolute deviations between experimental and theoretical values are 15 and 20 cm^{-1} for the B3LYP and RHF calculations, respectively. In this case, DFT method provided more accurate vibrational spectra than the RHF method. Hence, the mode description provided with band assignments here is based on the B3LYP calculations.

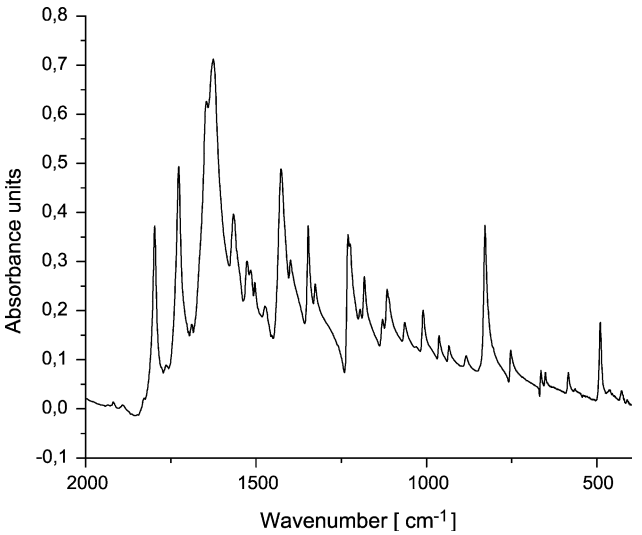

Fig. 2. Infrared spectrum of DAPB (1 mg in 200 mg KBr) in 2000–400 cm^{-1} frequency region.

The molecule of DAPB has C_{2v} symmetry. As a result, DAPB possesses 72 normal vibrations distributed in:

$$\Gamma = 24A_1 + 10A_2 + 15B_1 + 23B_2.$$

All bands are Raman and IR active except for A_2 symmetry class forbidden in the IR spectrum.

Assignments of the bands in the experimental spectrum are carried out on the basis of previous work for PBSQ [9] as well as calculations presented here.

4.3. Vibrational assignment of dimethylaminopyridinium moiety

Four stretching modes of pyridinium ring ν(CH) viz. **2**, **20a**, **7** and **20b** were observed in the IR spectrum of DAPB. The calculated frequencies by B3LYP are significantly

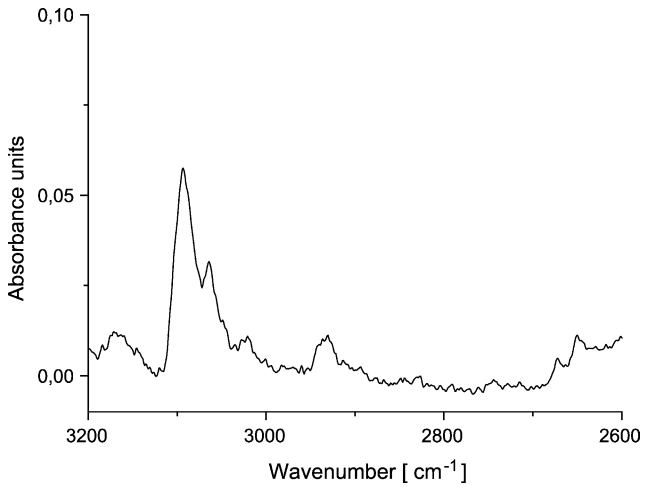

Fig. 1. Infrared spectrum of DAPB (1 mg in 200 mg KBr) in 3200–2600 cm^{-1} frequency region.

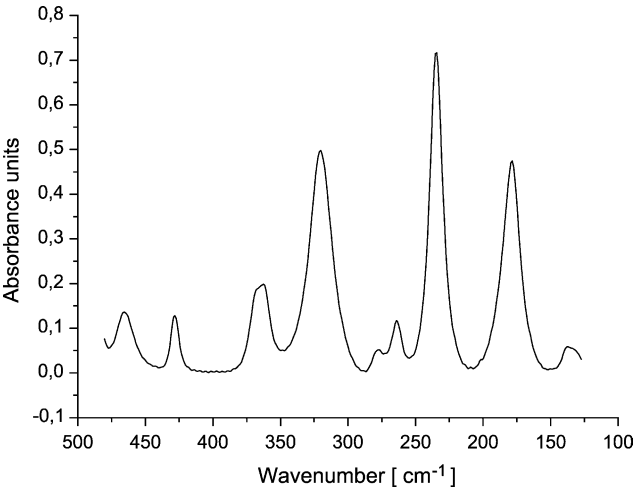

Fig. 3. Infrared spectrum of DAPB (6 mg in 200 mg CsI) in 400–100 cm^{-1} frequency region.

Table 3
Theoretical and experimental (nujol/perdeuteronujol) vibrational frequencies ν (cm^{-1}) intensities A (km mol^{-1}) of DAPB molecule

No.	B3LYP		RHF		Experimental	Character[a]	
	ν^b	A	ν^c	A	ν		
1.	3130	0.3	3092	10.6	3094	$\nu_{Py}(CH)$	**2**
2.	3129	9.1	3067	0.3	3068	$\nu_{Py}(CH)$	**20a**
3.	3096	9.2	3065	9.4	3064	$\nu_{Py}(CH)$	**7**
4.	3095	11.3	3046	12.7	3048	$\nu_{Py}(CH)$	**20b**
5.	3056	23.4	3010	41.2	3010	$\nu_{Me}(CH)$	
6.	3044	1.2	2993	1.8	3000	$\nu_{Me}(CH)$	
7.	2972	46.1	2930	61.3	2930	$\nu_{Me}(CH)$	
8.	2971	0.0	2924	0.0		$\nu_{Me}(CH)$	
9.	2924	68.1	2876	33.7	2926	$\nu_{Me}(CH)$	
10.	2919	54.2	2869	57.0	2890	$\nu_{Me}(CH)$	
11.	1796	600.6	1865	745.6	1798	$\nu(C{=}O)$	
12.	1770	261.7	1805	68.8	1729	$\nu^s(C{=}O)$	
13.	1664	734.3	1672	1316.8	1644	$\nu^{as}(C{=}O)$	
14.	1642	322.7	1648	583.7	1635	$\nu_{Py}(CC)$, $\delta_{Py}(CCH)$	**8a**
15.	1525	590.3	1537	37.3	1568	$\nu_{Py}(CC)$, $\delta_{Py}(CCH)$	**8b**
16.	1501	3.7	1527			$\delta_{Py}(CCH)$, $\nu(C^4-N^{13})$	
17.	1494	27.6	1498	1.1	1517	$\delta_{Py}(CCC)$, $\delta_{Py}(CCH)$, $\delta_{Me}(HCH)$	**19a**
18.	1492	2.8	1492			$\delta_{Sq}(CCO)$, $\delta_{Py}(CCC)$	
19.	1472	0.2	1475	6.5	1474	$\delta_{Py}(CCC)$, $\delta_{Py}(CCH)$, $\delta_{Me}(HCH)$	**19b**
20.	1464	15.3	1472	13.4	1470	$\delta_{Me}(HCH)$, $\delta_{Py}(CCC)$	
21.	1455	0.0	1463	0.0		$\delta_{Me}(HCH)$, $\delta_{Py}(CCC)$	
22.	1451	143.8	1460	147.2		$\delta_{Me}(HCH)$, $\delta_{Py}(CCC)$	
23.	1418	0.5	1429	4.2	1425	$\delta_{Me}(HCH)$	
24.	1399	0.6	1421	29.8	1398	$\nu(C^7-N^1)$, $\nu_{Sq}(CC)$	
25.	1365	298.3	1377	411.7	1348	$\nu(C-N^{13})$, $\nu(N^{13}-C^{Me})$	
26.	1337	29.2	1354	32.5	1327	$\delta_{Py}(CCH)$	**3**
27.	1301	2.6	1269			$\nu(N^{13}-C^{Me})$, $\nu_{Py}(CC)$	
28.	1223	33.3	1217	221.7	1227	$\delta_{Py}(CCH)$	**9a**
29.	1211	44.0	1213		1196	$\nu_{Sq}(CC)$	
30.	1184	26.7	1178		1182	$\delta_{Me}(HCH)$	
31.	1168	6.4	1173	40.7		$\delta_{Py}(CCH)$, $\nu_{Py}(CC)$	**9b**
32.	1108	0.0	1123		1130	$\delta_{Py}(CCC)$, $\delta_{Sq}(CCO)$, $\nu_{Py}(CC)$	
33.	1107	0.1	1120			$\delta_{Me}(HCH)$	
34.	1100	7.7	1113		1115	$\delta_{Me}(HCH)$	
35.	1099	7.0	1110	45.7		$\delta_{Py}(CCC)$, $\nu_{Sq}(CC)$	**15**
36.	1048	24.3	1049	13.1	1063	$\nu(N^{13}-C^{Me})$, $\delta_{Me}(HCH)$	
37.	1007	26.0	1036	0.0		$\tau_{Py}(CCCH)$	**18a**
38.	968	0.0	1027	1.8	1025	$\tau_{Py}(CCCH)$	**18b**
39.	967	4.9	1013	41.9	1010	$\delta_{Py}(CCC)$, $\nu_{Py}(CC)$	**1**
40.	930	34.7	1005	79.3	964	$\delta(CCN^1)$, $\delta_{Sq}(CCC)$	**5**
41.	919	42.7	929	19.4	934	$\delta_{Py}(CCC)$, $\nu_{Py}(CC)$, $\nu(N^{13}-C^{Me})$	
42.	846	4.7	855	3.5	883	$\nu_{Sq}(CC)$, $\delta_{Sq}(CCC)$	
43.	815	60.6	838	99.8	829	$\tau_{Py}(CCCH)$	**10a**
44.	808	0.0	828	0.0		$\tau_{Py}(CCCH)$	**10b**
45.	777	2.2	794	1.8	789	$\delta_{Sq}(CCO)$	
46.	746	1.7	764	8.0	754	$\tau_{Sq}(CCCO)$	
47.	741	3.6	739	9.1		$\delta_{Py}(CCC)$, $\nu(N^{13}-C^{Me})$	
48.	702	0.6	724	2.4		$\tau_{Py}(CCCC)$	**4**
49.	644	0.1	645	0.2	664	$\delta_{Py}(CCH)$	**11**
50.	626	0.1	639	3.8	651	$\delta_{Py}(CCC)$, $\nu_{Sq}(CC)$	
51.	584	0.0	616	0.0	584	$100\tau_{Sq}(CCCO)$	
52.	575	5.1	570	7.0	570	$\tau_{Py}(CCCN)$	
53.	534	1.6	536	2.0		$\tau_{Py}(CCCC)$, $\tau(CCC-N^{13})$, $\tau_{Py}(CCCH)$	
54.	478	2.7	477	3.1	492	$\delta(N^{13}CC)$, $\delta(CN^{13}C)$	
55.	467	13.6	473	35.8	475	$\delta(CN^{13}C^{Me})$	**16a**
56.	444	0.2	444	0.4	465	$\tau_{Py}(CCCN)$	
57.	418	0.0	421	0.0	450	$\delta_{Sq}(CCO)$, $\delta(CCN^1)$	
58.	342	0.4	345	29.3	362	$\delta(CN^{13}C^{Me})$, $\delta(CCN^1)$	
59.	336	17.9	344	0.5	320	$\tau_{Py}(CCCH)$	**16b**

(*continued on next page*)

Table 3 (*continued*)

No.	B3LYP		RHF		Experimental	Character[a]
	ν^b	A	ν^c	A	ν	
60.	311	12.9	320	23.5		τ_{Py}(CCCC), τ_{Py}(N^1CCC), τ_{Sq}(CCCO)
61.	249	1.4	266	2.8	264	δ_{Sq}(CCO), δ_{Sq}(CCC)
62.	225	0.1	239	0.1	236	τ_{Py}($C^9C^7N^1C^2$), δ_{Me}(HCH)
63.	216	11.7	220	14.6		ν(N^1-C^7), δ_{Sq}(CCC)
64.	205	0.2	209	0.2		δ($CN^{13}C$), δ($N^{13}CC$)
65.	181	0.0	193	0.0	178	τ_{Py}(CNCH)
66.	151	7.8	150	6.1	138	τ($N^1C^7C^8C^9$), τ_{Py}(CCCC)
67.	95	1.0	108	7.4		τ($CN^{13}CC$), τ(CCN^1C)
68.	89	0.0	87	0.1		τ_{Sq}(CCCC), τ_{Sq}(CCCO)
69.	81	0.3	85	0.6		δ($C^7N^1C^2$), δ($C^7C^8N^1$)
70.	80	1.7	78	0.0		τ(CCN^1C), τ_{Py}(HCNC)
71.	56	0.0	44	0.0		τ_{Sq}(CCN^1C^2), τ_{Sq}($CCCN^1$)
72.	42	0.4	41	0.6		τ_{Sq}($C^{Me}N^{13}CC$), τ($C^9C^7N^1C^2$)

[a] From B3LYP calculations. Vibrational modes: ν, stretching; δ all type of deformations, respectively; τ, torsion. Wilson's notation is used for the phenyl modes.
[b] Scaled by 0.8953 [17].
[c] Scaled by 0.9614 [17].

higher since as known DFT methods lead to overestimating of C–H stretching frequencies [21]. The agreement, however, of RHF\6-31G* calculated frequencies with the experimental data is very good in this region (the mean deviation between experimental and calculated data is about 2 cm^{-1}).

The six modes ($\nu_5-\nu_{10}$) corresponding to the symmetric and the asymmetric C–H stretching of the methyl groups are in the frequency region of 3010–2890 cm^{-1}. RHF calculation predicted them in the frequency region of 3010–2870 cm^{-1}. The band ν_8, which is predicted as inactive in IR spectrum (A_2 symmetry) misses in the experimental spectrum. Both in the experiment and calculations, from weak to medium IR intensity is observed for these bands.

The normal vibrations of predominantly ring C–C stretching character viz. **8a**, **8b**, **19a** and **19b** have been predicted quite correctly by both B3LYP and RHF methods (the mean absolute deviation is 10 and 12 cm^{-1}, respectively). The most intensive band in the experimental IR spectrum of DAPB at 1626 cm^{-1} was assigned to vibration **8a**. The frequency of this mode is well predicted by B3LYP method (1642 cm^{-1}) and by RHF (1648 cm^{-1}). It's too high intensity is obviously due to vibronic coupling in the molecule studied. The very strong bands in IR spectra in this frequency region and the resonantly enhanced bands in the IR and Raman spectra mainly correspond to vibrations having a form of transition between aromatic-like and quinone-like structure [22]. Among them especially the phenyl vibration **8a** in the frequency region 1580–1620 cm^{-1} is often observed in the IR spectra of radical ions generated from aromatic ketones [23]. On the other hand, high NLO efficiency of radical ions has been reported by Meerholz et al. [24]. Hence, our assignment is in a good agreement with the literature data [9]. The C–H in-plane deformation vibrations: **3**, **9**, **18a**, **18b** in the experimental spectrum are found in the frequency region of 1326–1025 cm^{-1}, which is in agreement with the theoretical data (Table 3). The in-plane normal mode **18a** predicted at 1036 cm^{-1} (RHF), 1007 cm^{-1} (B3LYP) is not observed in the experimental spectrum (A_2 mode).

The frequency of the normal mode **1** ('breathing') is predicted fairly well by theory: calculated 1013 (B3LYP), measured 1010 cm^{-1}. The predicted character of this normal mode is predominantly δ_{CCC} ring deformation (Table 3).

The frequency region of C–H out-of-plane deformation vibrations **5**, **10a**, **10b** and **11** is predicted correctly: calculated 1005–645 cm^{-1} (B3LYP), measured 964–664 cm^{-1}.

The deformation vibrations of the pyridinium ring **4**, **6**, **16b** and **16a** are predicted in the frequency region of 724–344 cm^{-1} (RHF) and 702–336 cm^{-1} (B3LYP). At the RHF and B3LYP levels, well-known problems mainly concern the frequencies of **4** and **14** modes (Wilson's notation). Whereas the frequency of **4** mode seems to be reliable 724 cm^{-1} (RHF), 702 cm^{-1} (B3LYP), but we cannot find the band in this region in the experimental spectrum. The calculated band has a very low intensity (2.4 km mol^{-1}) and this could be the reason for its absence in the experimental IR spectrum. Failure with a correct description of the 'Kekule' type mode has evidently basic reason [25]. Besides, even with large basis sets the overall correspondence with the experimental data remains poor. A good agreement between the computed and the experimental frequencies of these modes is found in accordance with literature data for similar systems [26–28].

4.4. Vibrational assignment of squaric acid moiety

Stretching vibrations corresponding to the carbonyl groups are expected for the DAPB structure given above. The strong band at 1797 cm^{-1} can be predominantly assigned as stretching vibration of pure carbonyl group, $\nu(C_{10}{=}O_{17})$, while the two bands at 1726 and 1644 cm^{-1} correspond to the symmetric and asymmetric stretching vibrations of the two mutually connected oscillators C_8O_{16} and C_9O_{18}. The B3LYP/6-31G* method reproduces very well the frequency of the C=O stretching mode (the difference between the measured and the scaled calculated value is only 1 cm^{-1}), but overestimates significantly the frequency of ν^s(C=O) (with 44 cm^{-1}) and moderately the frequency of ν^{as}(C=O) (with 15 cm^{-1}) (Table 3). In both experimental and predicted IR spectra the carbonyl bands are very intensive. The frequency of the pure ν^s(C=O) vibration decreases slightly from 1792 cm^{-1} in PBSQ to 1798 cm^{-1} in this case. The band at 1762 cm^{-1} belonging to the mode ν^s(C=O) decreases its frequency to 1726 cm^{-1} while the band at 1697 cm^{-1} undergoes a frequency decrease to 1644 cm^{-1}. The bands of the two 'semi-carbonyl' groups regularly decrease their frequencies and increase their intensities as a result of the presence of 4-dimethylamino group. The behavior of the C=O groups is in accordance with the concept for the influence of different substituents on the carbonyl frequencies and intensities [29], while the behavior of the pure C=O group is in contrast with it. A possible explanation of this phenomenon could be looked for in the increase in vibrational interaction between these groups. Juchnovski et al. [30] have observed similar 'resonance-induced intensity borrowing' from ν(CO) bands to skeletal ones.

The band at 1398 cm^{-1} (predicted at 1399 (B3LYP), 1421 cm^{-1} (RHF)) corresponds primarily to stretching vibration with a small component of motion corresponding to the CC stretch of Sq. In-plane deformation of Sq moiety: found at 883 cm^{-1}, is predicted fairly well—855 cm^{-1} (RHF), 846 cm^{-1} (B3LYP). The band at 789 cm^{-1} in the experimental spectrum was assigned to in-plane vibration of the pure carbonyl group while the band at 754 cm^{-1} is described as mixed deformation vibration with predominantly CCCO character. The band at 584 cm^{-1} can be assigned to out-of-plane deformation vibration of the C=O bond. The remaining part of the vibrations of Sq moiety is coupled with the vibrations of the pyridinium part. The band predicted at 205 cm^{-1} (DFT) and 209 cm^{-1} (RHF) having purely C–N–C and N–C–C character of Sq moiety was not found in the experimental spectrum.

5. Conclusions

The bands of IR spectrum of DAPB were assigned with the help of force field calculations. The majority of the experimental frequencies are very well reproduced by the B3LYP/6-31G* method, and well by the RHF/6-31G*. The comparison of the theoretical with the experimental spectra provides important information about the ability of these computational methods to describe the vibrational modes in this highly polar strained ring compound.

On the basis of the charge distribution analysis it is concluded that in the isolated DAPB molecule the Sq moiety plays the role of electron donor and the pyridinium group of electron acceptor. Influence of dymethylamino group on the frequencies and intensities is clearly distinct and it is predicted well from the theoretical method used. The very high dipole moment of the DAPB molecule responsible for the extremely high melting point (with decomposition) is predicted well from theory. It is found that the structure of DAPB is an intermediate structure between the aromatic-like and the quinoid-like one.

Acknowledgements

We thank the DAAD—Bonn, Germany for a grant within the priority programme 'Stability Pact for South Eastern Europe', Bulgarian National Fund of Scientific Research, Contract X-1213. One of us (Ts.K.) thanks the Alexander von Humboldt Stiftung—Bad Godesberg (Germany) for financial support.

References

[1] D. Chemla, J. Zyss (Eds.), Nonlinear Optical Properties of Organic Molecules and Crystals, vols. 1 and 2, Academic Press, New York, 1987.
[2] T. Watanabe, H. Nalwa, S. Miyata (Eds.), Nonlinear Optics of Organic Molecules and Polymers, CRC Press, Boca Raton, 1997, Chapter 3. H. Nalwa, S. Miyata (Eds.), Nonlinear Optics of Organic Molecules and Polymers, CRC Press, Boca Raton, 1997, Chapter 4.
[3] J.J. Wolff, R. Wortmann, Organic Materials for Second-Order Nonlinear Optics, Advances in Physical Organic Chemistry, vol. 32, 1999, p. 121.
[4] S. Marder, J. Perry, W. Schaefer, Science 245 (1989) 626.
[5] S. Marder, J. Perry, C. Yakymyshyn, Chem. Mater. 6 (1994) 1137.
[6] C.B. Gorman, S.R. Marder, Chem. Mater. 7 (1995) 215.
[7] M. Szafran, J. Koput, J. Mol. Struct. 381 (1996) 157.
[8] M. Viertorinne, J. Valkonen, I. Pitkanen, M. Mathlouthi, J. Nurmi, J. Mol. Struct. 477 (1999) 23.
[9] Ts.M. Kolev, D.Y. Yancheva, B.A. Stamboliyska, Spectrochim. Acta, Part A 59 (2003) 1805.
[10] A. Schmidt, U. Becker, A. Aimene, Tetrahedron Lett. 25 (1984) 4475.
[11] A. Schmidt, A. Aimene, M. Schneider, Synthesis (1984) 436.
[12] A. Schmidt, M. Schneider, A. Aimene, M. Straus, D. Botzet, Chem. Zeit. 109 (1985) 333.
[13] Ts. Kolev, D. Yancheva, St. Stoyanov, Advanced Functional Materials, submitted for publication.
[14] M.J. Frisch, G.W. Trucks, H.B. Schlegel, G.E. Scuseria, M.A. Robb, J.R. Cheeseman, V.G. Zakrzewski, J.A. Montgomery, Jr., R.E. Stratmann, J.C. Burant, S. Dapprich, J.M. Millam, A.D. Daniels, K.N. Kudin, M.C. Strain, O. Farkas, J. Tomasi, V. Barone, M. Cossi, R. Cammi, B. Mennucci, C. Pomelli, C. Adamo, S. Clifford, J.

Ochterski, G.A. Petersson, P.Y. Ayala, Q. Cui, K. Morokuma, D.K. Malick, A.D. Rabuck, K. Raghavachari, J.B. Foresman, J. Cioslowski, J.V. Ortiz, A.G. Baboul, B.B. Stefanov, G. Liu, A. Liashenko, P. Piskorz, I. Komaromi, R. Gomperts, R.L. Martin, D.J. Fox, T. Keith, M.A. Al-Laham, C.Y. Peng, A. Nanayakkara, C. Gonzalez, M. Challacombe, P.M.W. Gill, B. Johnson, W. Chen, M.W. Wong, J.L. Andres, C. Gonzalez, M. Head-Gordon, E.S. Replogle, J.A. Pople, GAUSSIAN 98, Revision A.7, Gaussian, Inc., Pittsburgh PA, 1998.

[15] A.D. Becke, J. Chem. Phys. 98 (1993) 5648.

[16] C. Lee, W. Yang, R.G. Parr, Phys. Rev. B 37 (1988) 785.

[17] A.P. Scott, L. Radom, J. Phys. Chem. 100 (1996) 16502.

[18] Ts. Kolev, D. Yancheva, D.Chr. Kleb, M. Schürmann, H. Preut, M. Spiteller, Acta Crystallogr. Sect. E 58 (2002) o1267.

[19] M.J.G. Lesley, A. Woodwared, N.J. Taylor, T.B. Marder, I. Gazenobe, I. Ledoux, J. Zyss, A. Thornton, D.W. Bruce, A.K. Kakkar, Chem. Mater. 10 (1998) 1355.

[20] E.B. Wilson, Phys. Rev. 45 (1934) 427.

[21] A.A. El-Azhary, H.U. Suter, J. Phys. Chem. 100 (1996) 15056.

[22] M. Szostak, T. Misiaszek, R. Roszak, J. Rankin, R. Czernuszewicz, J. Chem. Phys. 99 (1995) 14992.

[23] I. Juchnovski, Ts. Kolev, Spectrosc. Lett. 18 (1985) 481. I. Juchnovski, Ts. Kolev, Spectrosc. Lett. 18 (1985) 471.

[24] K. Meerholz, J. Swiatkiewicz, P. Prasad, J. Chem. Phys. 99 (1995) 7715.

[25] H. Lampert, W. Mikenda, A. Karpfen, J. Phys. Chem. A101 (1997) 2254.

[26] Ts. Kolev, B.S. Stambolyska, Spectrochim. Acta, Part A 56 (1999) 119.

[27] Ts. Kolev, B.S. Stambolyska, Spectrochim. Acta, Part A 59 (2003) 3127.

[28] G. Varsanyi, S. Szoeke, Vibrational Spectra of Benzene Derivatives, Academic Press, New York, 1969.

[29] Ts. Kolev, Vibrational and structural investigation of some mono and diketones-potential materials for non-linear optics, Doctor of Science Theses, Institute of Organic Chemistry, Bulgarian Academy of Sciences, Sofia, 2001.

[30] I. Juchnovski, Ts. Kolev, I. Binev, Spectrosc. Lett. 14 (1981) 763.